Polymer Vol. 39 No. 13, pp. 2725–2732, 1998

0032-3861/98/$19.00+0.00

PII: S0032-3861(97)00620-4

# $^2$H n.m.r. analysis of the phenylene motion in different poly(ethylene terephthalate) samples

**Takahiro Kawaguchi[a,*], Akira Mamada[a], Yasunori Hosokawa[a] and Fumitaka Horii[b]**

[a]*Chemicals and Materials Research Laboratories, Kao Corporation, 1334 Minato, Wakayama 640, Japan*

[b]*Institute for Chemical Research, Kyoto University, Uji, Kyoto 611, Japan*

*(Received 24 June 1997; accepted 25 July 1997)*

The detailed characterization of the phenylene motions in phenylene-deuterated poly(ethylene terephthalate) (PET) samples has been performed at different temperatures by solid-state $^2$H n.m.r. spectroscopy. Samples used are slowly cooled PET, quenched PET, and quenched PET containing 10 wt% bisphenol-A. $^2$H spin-lattice relaxation analyses reveal that there exist three components with different $T_1$ values at each temperature in each sample, which can be assigned to the crystalline, less mobile noncrystalline, and mobile noncrystalline components in the order of decreasing $T_1$ value. Using these differences in $T_1$, $^2$H n.m.r. spectra of the respective components are separately recorded, and they are compared to the simulated spectra obtained by the two-site 180° flip model for the motion of the phenylene group. As a result, it is found that the $^2$H n.m.r. spectra are successfully reproduced for the respective components by introducing the individual characteristic log-Gaussian distributions in the flip rates. Moreover, the mass fractions of the respective components are determined for each PET sample as a function of temperature. On the basis of these results, the features of the phenylene motions are discussed, particularly in the noncrystalline regions. 

**(Keywords: solid state $^2$H n.m.r.; poly(ethylene terephthalate); molecular motion)**

## INTRODUCTION

Poly(ethylene terephthalate) (PET) is one of the most important plastics in chemical industries because of its extensive use for bottles, fibres, films, and different parts of machines. In such wide uses PET may be indebted to the excellent properties for transparency, gas barrier ability, thermal expansion coefficient, flatness and so on, but many efforts are still being made to improve the physical properties for a higher performance material.

To gain a clue for further improvement of the physical properties of this polymer, it is necessary to study the solid-state structure and molecular motions in detail. Previously $^1$H and $^{13}$C n.m.r. have been used to assess the nature of the molecular motions for PET[1–7]. For example, reorientations of the ethylene and phenylene groups were investigated[1], and four separate motional processes were distinguished[2]; rapid small angular fluctuations, a slower motion that is unique to the ethylene groups (probably *trans–gauche* isomerization), a specific motion of the phenylene ring (possible flipping), and an almost effectively isotropic reorientation of some amorphous polymer segments. Furthermore, it was found that the phenylene flip motion starts at room temperature[3] and its isotropic motion also becomes possible at lower temperatures than that of the ethylene group[4].

Solid-state $^2$H n.m.r. spectroscopy is well suited for determining modes and frequencies of local molecular motions of different components included in solid polymers, because this technique has a number of advantages. First, the sample can be selectively deuterated so that specific sites of interest are observed. Second, the quadrupole interaction between the spin $I = 1$ deuterium nucleus and the electric field gradient of the C–D bond dominates the spectrum. Third, the shape of the quadrupole spectra are sensitive to orientation in the sample and to molecular motion involving the C–D bond. For example, previous investigations show that poly(butylene terephthalate)[8] contains three distinct motional regimes consisting of the crystalline, intermediate mobility, and amorphous regions: the phenylene rings undergo, respectively, slow 180° flip motions or more rapid 180° flips superimposed on rapid librational motion in the inter-phase or amorphous region, whereas those rings are static in the crystalline region on the $^2$H n.m.r. time scale. It is also found that in PET the phenylene flip motion begins well below the glass transition temperature while the *trans–gauche* jump motion of the ethylene units is still restricted at that temperature[9].

However, molecular motions of the respective phases of solid polymers are not always described by a single correlation time for a single type of motion. The molecular dynamics of nylon 66 was extensively characterized by $^2$H n.m.r. line shape analysis combined with spin-lattice relaxation experiments and wide distributions of angles of librational motions were determined for the constituent methylene carbons in the crystalline and noncrystalline regions[10,11]. On the other hand, distributions of correlation times or flip angles were found for the phenylene flip motion in bisphenol-A polycarbonate by $^2$H n.m.r. spectra[12,13] or $^{13}$C chemical shift anisotropy[14] analyses.

Compared with cases of nylon 66 and polycarbonate, PET has not been characterized in detail by $^2$H n.m.r. despite the importance of this material as described above. In this paper we present a detailed investigation of the phenylene flip

* To whom correspondence should be addressed

motion in partially deuterated semicrystalline PET samples by a $^2H$ n.m.r. line shape analysis. Distributions of correlation times in the crystalline and noncrystalline regions can be separated by using differences in spin-lattice relaxation times. This analytical method is applied for the characterization of the phenylene motion in PET samples prepared under different conditions.

## EXPERIMENTAL SECTION

### *Samples*

Phenylene-ring deuterated PET was synthesized as follows: deuterated terephthalic acid (0.1 mol) and ethylene glycol (1.0 mol) were directly reacted in a flask at 200–230°C for about 5 h in a $N_2$ atmosphere. Next the system was evacuated at 200–230°C for 5 h and then kept at 270°C in vacuo for about 3 h. The product was extracted with hexafluoroisopropanol for purification, and dried in vacuo at 60°C for about 9 h. The viscosity-average molecular weight of this sample was estimated to be 7700 by using phenol/1,1,2,2-tetrachloroethane (60/40 wt. ratio) as solvent.

A part of the PET sample thus obtained was pressed into films with a thickness of about 200 nm at room temperature after pouring the sample melted at 280°C into a mould left at room temperature. This specimen is referred to as quenched PET film (QCD) hereafter, although the degree of crystallinity estimated by wide-angle X-ray diffractometry is as high as about 0.20, as described later, because of insufficient quenching. In contrast, slowly cooled PET films (SCD) were pressed at 280°C in the melted state and then cooled to room temperature spontaneously. Other quenched PET films containing bisphenol-A (QBPA) were prepared in a similar way to the case of QCD for the PET sample mixed with 10 wt% bisphenol-A at 280°C.

### *$^2H$ n.m.r. measurements*

Solid-state $^2H$ n.m.r. measurements were performed on a JEOL JNM-GX4OO spectrometer equipped with a JEOL variable temperature $^2H$ n.m.r. probe operating at 61.25 MHz under a static magnetic field of 9.4 T. Fully relaxed spectra were acquired with a standard quadrupolar echo pulse sequence, where the $\pi/2$ pulse width and the delay time were 3.1 and 20 $\mu$s, respectively. Spin-lattice relaxation behaviour was measured at each temperature by the saturation recovery method to separate the contributions from the crystalline and noncrystalline regions. The temperatures of samples were calibrated by using a thermocouple

### *Simulations of $^2H$ n.m.r. spectra*

Simulated $^2H$ n.m.r. spectra were obtained on a Stella Serge computer by the program originally prepared using the two-site exchange model[14–16]. The asymmetric parameter $\eta$ of the phenylene ring was determined to be 0.03 according to the method previously reported[17], The simulated spectra were corrected for the effects of pulse power fall-off[18] and for the effects of motions that occur during the quadrupolar echo delay time[19].

## RESULTS AND DISCUSSION

It has been found by d.s.c. and wide-angle X-ray diffraction measurements that each sample contains the crystalline component, although the degree of crystallinity depends on the preparation condition of each sample. Therefore, the $^2H$ n.m.r. spin-lattice relaxation process has been measured by the saturation recovery method to discriminate between the contributions from the crystalline and noncrystalline regions. *Figure 1* shows the saturation recovery process measured for QCD at 25°C, where the peak intensity at +15.5 kHz from the resonance center is plotted against the time for relaxation. Since this recovery curve is not described in terms of a single exponential relaxation, we assume the existence of three components of different $T_1$ values ($T_{1L}$, $T_{1M}$, $T_{1S}$). In this case the magnetization $M(t)$ at time $t$ should be expressed as follows;

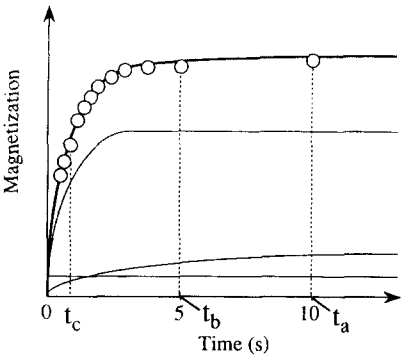


**Figure 1** $^2H$ spin-lattice relaxation recovery process obtained by the saturation recovery method for QCD at 25°C. Open circles are experimental data. The thick solid line is the composite line obtained by the least-squares method for the three components with different $T_1$ values, which are indicated as thin solid lines

$$M(t) = M_{S0}[1 - \exp(-t/T_{1S})] + M_{M0}[1 - \exp(-t/T_{1M})] + M_{L0}[1 - \exp(-t/T_{1L})] \quad (1)$$

where $M_{S0}$, $M_{M0}$ and $M_{L0}$ are the equilibrium magnetizations of the components with short, medium and long $T_1$ values, respectively. The simulated curve of equation (1), which is shown by a thick solid curve in *Figure 1*, is in good accord with the experimental data. As a result, the three $T_1$ values are determined as follows; $T_{1S}$ = 0.051 s, $T_{1M}$ = 0.99 s, $T_{1L}$ = 14 s. Almost the same $T_1$ values were also obtained by the same analysis for the spin-lattice relaxation processes of the peak intensity at ± 64 kHz from the resonance centre. On the basis of this fact, it is assumed that the anisotropy in $T_1$ may be negligibly small compared to the ratios between the respective $T_1$ values. Here, it is also assumed for a similar reason that there may be no significant effect of the spin diffusion on the $T_1$ analysis, particularly on the spectral editing of the different $T_1$ components which will be described below.

Using the same method, two or three $T_1$ values have been obtained for each sample from −30 to 130°C, which are plotted against the inverse absolute temperature in *Figure 2*. The respective $T_1$ values clearly decrease with increasing temperature for each sample. This trend suggests that the longer $T_1$ values are associated with less mobility; thus we simply assign the components with short, medium and long $T_1$ values to the mobile noncrystalline, less mobile noncrystalline, and crystalline components, respectively. This assignment will be confirmed later through the line shape analysis of the respective $^2H$ n.m.r. spectra.

With the use of such a large difference in $T_1$, we separate the total spectrum into the respective contributions as follows: According to equation (1), the magnetization at time $t_a$ is expressed as the following equation, when $t_a$ is five times longer than $T_{1M}$:

$$M(t_a) = M_{S0} + M_{M0} + M_{L0}[1 - \exp(-t_a/T_{1L})] \quad (2)$$

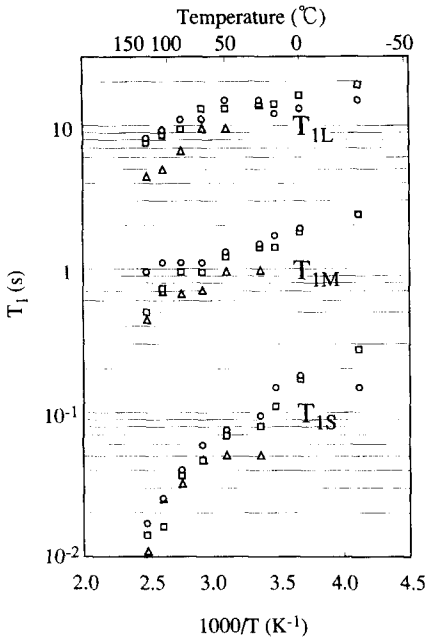


**Figure 2** Temperature dependences of the spin-lattice relaxation times ($T_1$) for the three components; △, QCD; □, SCD; ○, QBPA

Similarly the magnetization at time $t_b$ is

$$M(t_b) = M_{S0} + M_{M0} + M_{L0}[1 - \exp(-t_b/T_{1L})] \quad (3)$$

where it is assumed that $t_a > t_b > 5T_{1M}$.

By subtracting equation (3) from equation (2), the magnetization $M_L$ of the component with $T_{1L}$, which corresponds to the spectrum of the crystalline component, is given by

$$M_L = M(t_a) - M(t_b) = M_{L0}[\exp(-t_b/T_{1L}) - \exp(-t_a/T_{1L})] \quad (4)$$

For the purpose of separating the contributions of the components with $T_{1M}$ and $T_{1S}$, we need another magnetization at time $t_c$ described as

$$M(t_c) = M_{S0} + M_{M0}[1 - \exp(-t_c/T_{1M}) + M_{L0}[1 - \exp(-t_c/T_{1L})] \quad (5)$$

where $t_b > t_c > 5T_{1S}$. Then, by using equation (2), equation (3), and equation (5), we can separately obtain the magnetizations, $M_M$ and $M_S$, for the components with $T_{1M}$ and $T_{1S}$, which correspond to the spectra of the less mobile and mobile noncrystalline components, respectively, as follows:

$$M_M = B \cdot M(t_a) + (A - B) \cdot M(t_b) - A \cdot M(t_c) = AC \cdot M_{M0} \quad (6)$$

$$M_S = -(BD + CE) \cdot M(t_a) + [CE - (A - B)D] \cdot M(t_b) + A(C + D) \cdot M(t_c) = AC \cdot M_{S0} \quad (7)$$

Here,

$$A = \exp(-t_b/T_{1L}) - \exp(-t_a/T_{1L}) \quad (8)$$

$$B = \exp(-t_b/T_{1L}) - \exp(-t_c/T_{1L})$$

$$C = \exp(-t_c/T_{1M})$$

$$D = 1 - \exp(-t_c/T_{1M})$$

$$E = 1 - \exp(-t_c/T_{1L})$$

In real cases, however, the signal/noise ratios were seriously low for the less mobile component in each sample at different temperatures. Accordingly, the spectra of the total noncrystalline component $M_N$ are obtained by the following equation instead of $M_M$:

$$M_N = [(A - F)/A] \cdot M(t_a) + (F/A) \cdot M(t_b) = M_{S0} + M_{M0} \quad (9)$$

where,

$$F = 1 - \exp(-t_a/T_{1L}) \quad (10)$$

The spectra of the crystalline component obtained for QCD at 25–130°C by the subtraction based on equation (4) are shown in *Figure 3*. These spectra are almost unchanged in line shape with increasing temperature and resemble the rigid Pake pattern, suggesting that the phenylene motion is hindered in this temperature range. Since this fact reflects one of features of the crystalline component, the method of spectral separation seems to be supported in that a population of chains with low mobility is identified as the crystalline component.

*Figure 4* shows the $^2H$ n.m.r. spectra of the crystalline, total noncrystalline, and mobile noncrystalline components obtained by the method described above for QCD at 25°C. The corresponding simulated spectra are also shown in this figure. Here, a log-Gaussian distribution in the flip rate is assumed for the two-site phenylene flip motion in each component, where the flip angle is fixed to 180°. A satisfactory good fit is obtained using the least-squares method for the crystalline and mobile noncrystalline components by assuming a monomodal distribution for the flip rate. It should be noted here that the frequency distribution for the crystalline component seemingly covers the region below the slow limit (~900 Hz) of the molecular motion for $^2H$ n.m.r. line shapes owing to the assumption of the log-Gaussian distribution. Namely only a small amount of the crystalline component with frequencies higher than the slow limit contributes to the change in line shape from the rigid Pake pattern. As for the total noncrystalline component, a bimodal log-Gaussian distribution, incorporating both the contribution from the mobile noncrystalline component and the additional contribution from the less mobile noncrystalline component, is required in order to obtain good fit. Finally the total spectrum can be successfully reproduced by adding the crystalline and noncrystalline contributions in an appropriate ratio. The mass fractions of the respective components are determined as the integrated fractions of the corresponding distributions.

*Figures 5–7* show observed and simulated spectra obtained at different temperatures for QCD, SCD, and QBPA, respectively. Log-Gaussian distributions of the flip rate for the three components, which are obtained as a result of the spectral simulations, are also shown at each temperature in these figures. It is found that the simulated spectra agree well with the observed spectra for these samples at the respective temperatures except for the results at 130°C. At lower temperatures, as seen in *Figures 6 and 7*, the crystalline and less mobile noncrystalline components are superposed with each other in the distribution of the flip rate. However, a small amount of the mobile noncrystalline component still exists, with a wide distribution of the flip rate even at −30°C. With increasing temperature, the average flip rate, which is defined as a peak value in the distribution function, shifts to a higher frequency side for the less mobile component and the distribution becomes broader for each sample.

As for the mobile noncrystalline component, the average

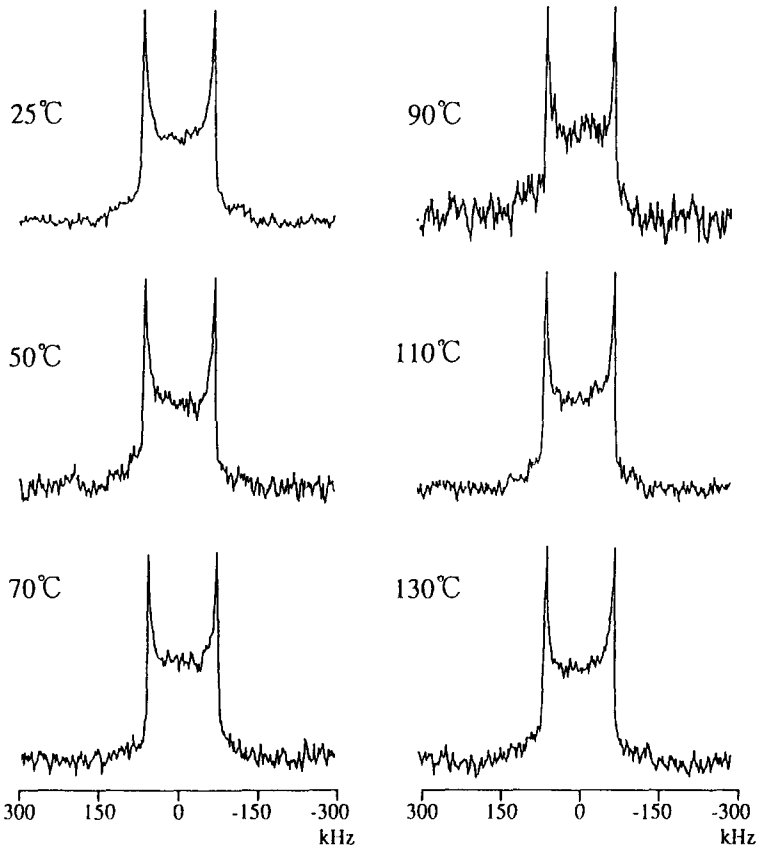


**Figure 3** $^2H$ n.m.r. spectra of the crystalline component for QCD at different temperatures

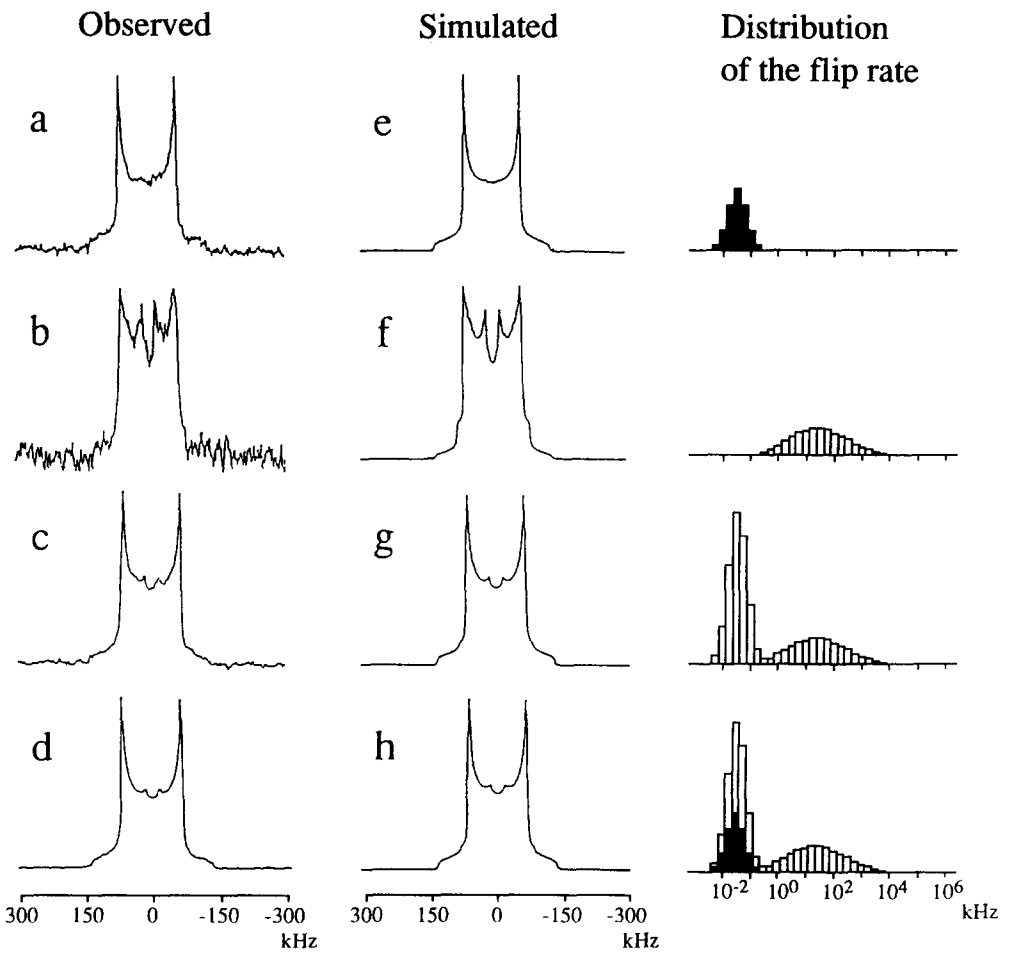


**Figure 4** Observed and simulated $^2H$ n.m.r. spectra for QCD at 25°C. (a,e) Crystalline; (b,f) mobile noncrystalline; (c,g) total noncrystalline; (d,h) total. The distributions of the rate of 180° flip motion are also shown in the respective cases on the right side of this figure

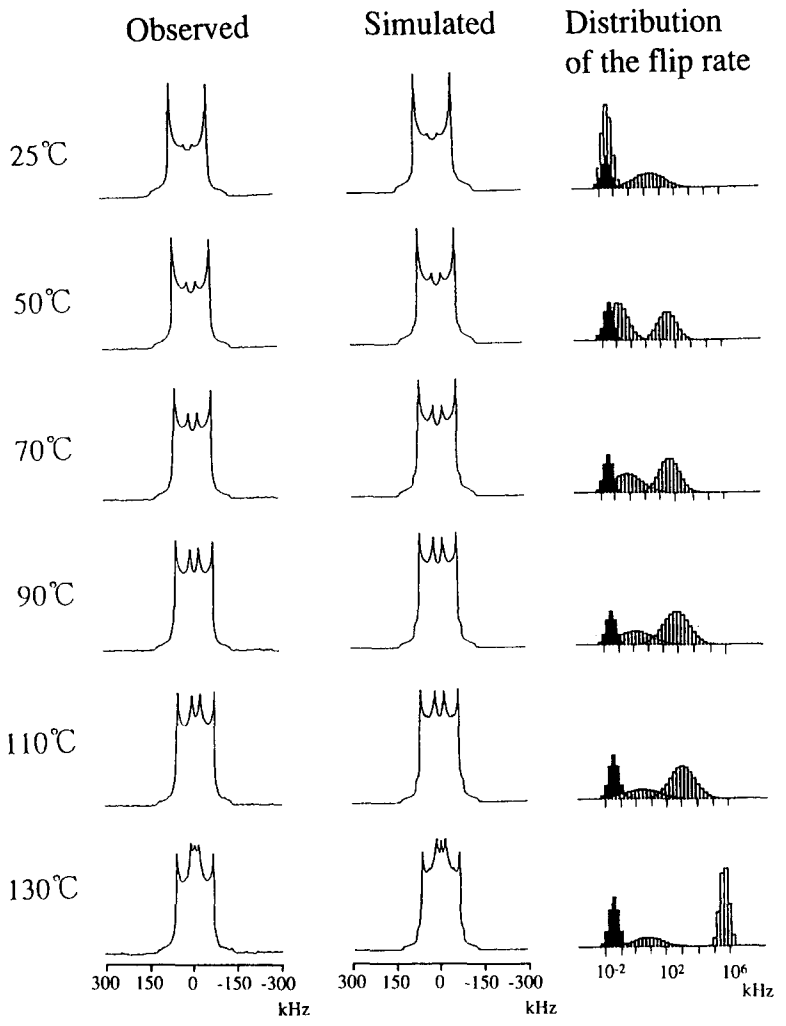


**Figure 5** Total observed and simulated $^2H$ n.m.r. spectra for QCD at different temperatures

flip rate also becomes higher with increasing temperature, but the width of the distribution becomes narrower. More drastic changes in the average flip rate and the distribution are recognized above 110 or 130°C; a much narrower distribution with a much higher average value appears for each sample. Moreover, an additional very sharp line, which is described by a Lorentzian curve, appears at the resonance centre at 130°C for each sample. This fact suggests the onset of the isotropic motion of the phenylene rings, because lower molecular weight compounds to possibly contribute to the sharp line may have been removed by the solvent extraction as described in the Experimental Section. Such a drastic change of the noncrystalline component may be associated with the glass-transition phenomenon detected through the motion of the phenylene rings. All these changes in line shape with temperature are found to be reversible except for the case of QCD, where an annealing effect appears as the increase in crystallinity during n.m.r. measurements at higher temperatures, as described later. It should be also noted here that the observed spectra for the mobile noncrystalline component are somewhat different in line shape at 130°C from the simulated spectra; in particular, the central contribution due to this component shown in *Figure 5* is significantly narrower than in the simulated spectrum. This may suggest the onset of the additional fluctuation of the flip axis of the phenylene ring.

Average correlation times $\bar{\tau}$ for the flip motion, which are obtained as inverse values of the average flip rates, are plotted against the inverse absolute temperature in *Figure 8* for the mobile and less mobile noncrystalline components in the respective samples. Here, the so-called slow and fast limits are also shown as broken lines, between which the line shape of the $^2H$ n.m.r. spectrum is significantly changed depending on the correlation time. Although some average correlation times for the less mobile component are greater than the slow limit, those values were able to be determined because some of the correlation times in their log-Gaussian distribution are less than the slow limit. These plots are not well described in terms of Arrhenius-type exponential functions $\bar{\tau} = \bar{\tau}_0 \exp(\Delta E/RT)$, but we estimate the activation energy for the flip motion from the slopes in the higher temperature side; $\Delta E$ = 77, 50, and 46 kJ/mol for the less mobile noncrystalline components and $\Delta E$ = 40, 24, and 40 kJ/mol for the mobile noncrystalline components in SCD, QCD, and QBPA, respectively. Since some parts of the two noncrystalline regions are interchangeable with each other depending on temperature, $\Delta E$ values for both components should be underestimated under this circumstance. Moreover, the increase of the degree of crystallinity by annealing may affect the $\Delta E$ value for QCD. Nevertheless, the order of $\Delta E$ values seems reasonable compared to reported values of 30–62 kJ/mol for phenylene motions in different BPA polycarbonates[13].

It should be noted here that the less mobile and mobile noncrystalline components can be successfully discriminated by the difference in flip rate. As described above,

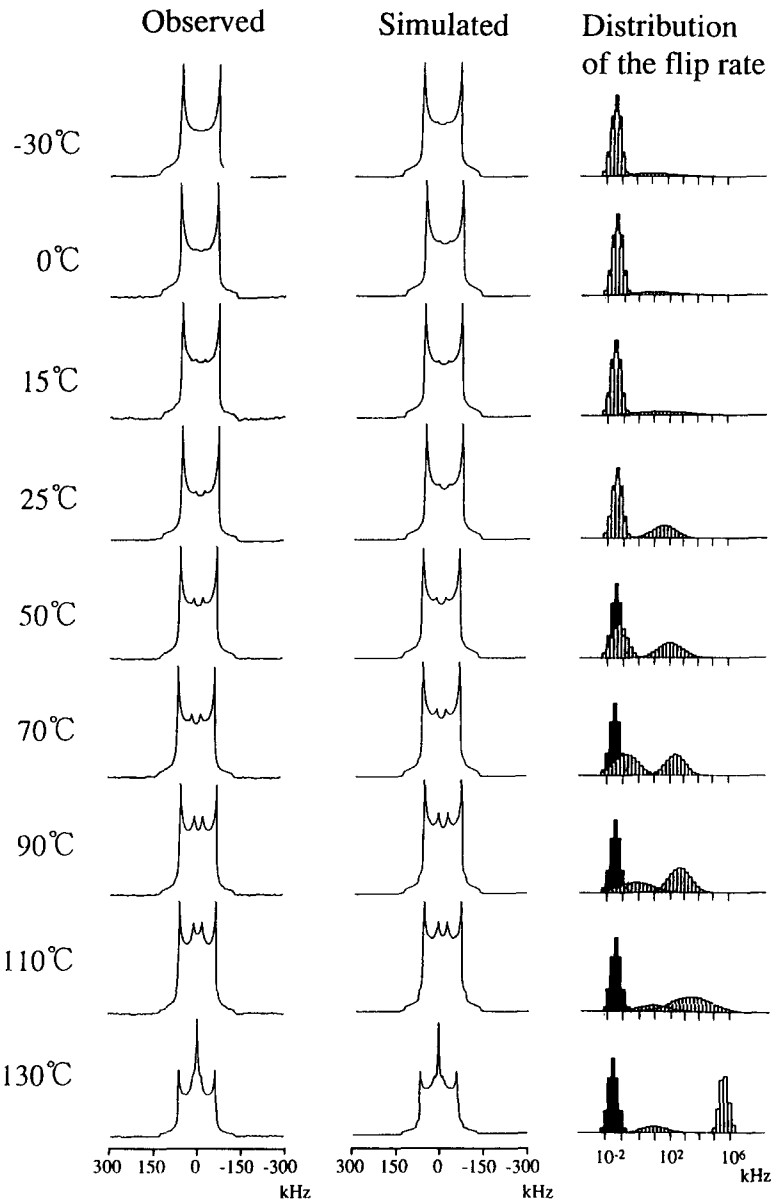


**Figure 6** Total observed and simulated $^2H$ n.m.r. spectra for SCD at different temperatures

these two components were originally separated by using the difference in $T_1$ which is sensitive to the molecular motion of the order of $10^8$ Hz. It is found from *Figure 8* that there is also a marked difference of 100–1000 Hz in flip frequency of the order of $10^2$–$10^7$ Hz between the two components. As for the content of each component, significant differences in the average correlation times for the less mobile noncrystalline component exist among the three samples. In particular, these values of QBPA are significantly longer than those of QCD, suggesting the higher hindrance of the phenylene motion in QBPA. Such low molecular mobility in QBPA may be due to the effect of the addition of BPA. When some amount of BPA is added in the preparation process of PET films, the gas barrier ability of the films is found to be much improved[20]. This will be closely associated to the low molecular mobility of the phenylene groups induced by the addition of BPA. A similar but smaller reduction of mobility is also recognized for the mobile noncrystalline component. On the other hand, the large temperature coefficient for the average correlation time, which corresponds to the larger activation energy, for the less mobile noncrystalline component of SCD is not clearly understood at present, but it may be associated with a less restricted chain conformation in the noncrystalline region for SCD, where the well phase-separated structure may be produced. This presumption is simply based on more enhancement in molecular mobility with increasing temperature for SCD.

*Figure 9* shows mass fractions of the respective components at different temperatures for each sample, obtained by the $^2H$ n.m.r. analysis described above. It is found that the crystalline, less mobile noncrystalline and mobile noncrystalline components exist in these samples at this temperature range. Although the mass fraction of the crystalline component slightly increases in QCD with increasing temperature, this value stays almost constant for SCD and QBPA. This result confirms the assignment that the longest $T_1$ component is the crystalline component. Moreover, it is suggested that some additional crystallization will be induced for QCD during n.m.r. measurements at higher temperatures. The degrees of crystallinity, which are defined as mass fraction of the

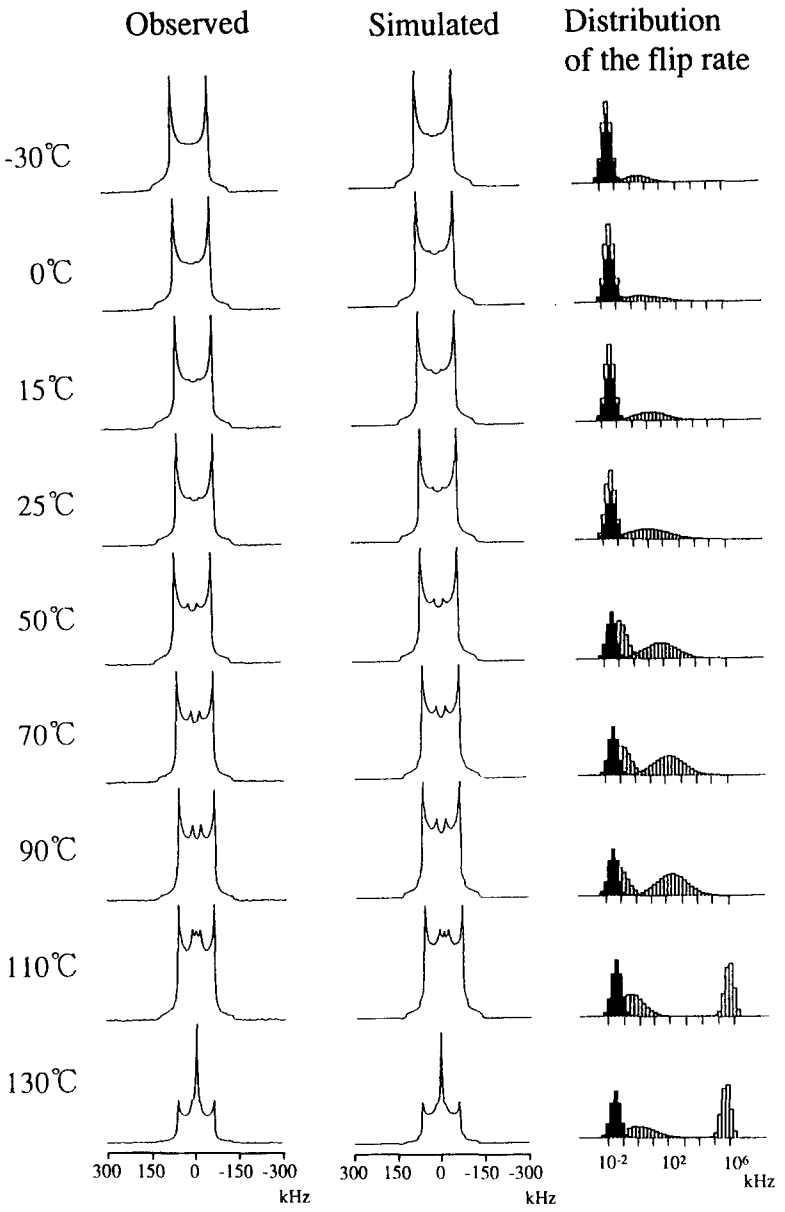


**Figure 7** Total observed and simulated $^2H$ n.m.r. spectra for QBPA at different temperatures

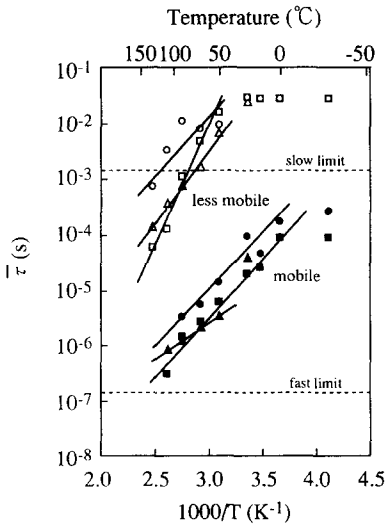


**Figure 8** Semilogarithmic plots of the average correlation times $\bar{\tau}$ of the flip motion, which are defined as inverse flip rates, for the less mobile and mobile components as functions of the inverse absolute temperature; △,▲, QCD; □,■, SCD; ○, ●, QBPA

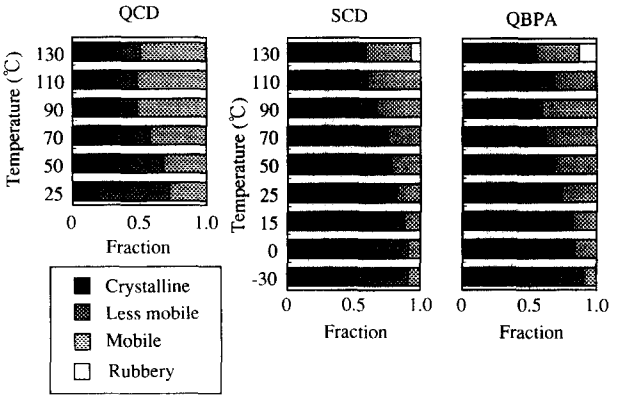


**Figure 9** Mass fractions of the respective components in QCD, SCD and QBPA at different temperatures obtained by the $^2H$ n.m.r. analysis

crystalline component at 25°C are 0.23, 0.47, and 0.31 for QCD, SCD, and QBPA, respectively. These values are in good accord with the degrees of crystallinities estimated by wide-angle X-ray diffractometry; 0.20 for QCD, 0.50 for

SCD, and 0.30 for QBPA. Such a remarkable decrease in crystallinity in QCD is due to the quenching effect of this sample. In contrast, QBPA has a significantly higher degree of crystallinity compared to QCD, although QBPA was prepared under the same conditions as for QCD. This result suggests that the addition of bisphenol-A may promote the crystallization of PET, probably by the increase of the growth rate due to the enhanced diffusion of PET segments. Higher $T_1$ values at higher temperatures for the crystalline component of QBPA, which are shown in *Figure 2*, may also indicate the production of more stable, larger-size crystallites in QBPA.

As for the less mobile and mobile noncrystalline components, their mass fractions markedly depend on the measurement temperature in these samples; some parts of the components are interchangeable as a result of the increase or the decrease in molecular mobility. At temperatures lower than −30°C the phenylene motion will be greatly hindered, leading to no discrimination between these two components. With increasing temperature, however, the phenylene groups belonging to segments with rather randomised conformation may start to contribute the mobile noncrystalline components. Therefore, the region close to the crystalline region will form the less mobile noncrystalline component, which may correspond to the interfacial region between the crystalline and amorphous regions. However, the detailed structure should be characterised by using spin diffusion measurements [21–23]. When the temperature increases further up to 110 or 130°C, the component with rubber-like mobility appears in SCD and QBPA. This component can be really assigned to the component with the random conformation with high mobility.

Finally, it should be noted that the fraction of the component with rubber-like mobility is highest for QBPA at 130°C. This result is in significant contrast to the lowest molecular mobility of the noncrystalline regions at lower temperatures as shown on QBPA in *Figure 8*. It may be reasonably concluded, therefore, that BPA plays a role as plasticizer above $T_g$, probably owing to the rapid phenylene flip motion, whereas it should be an antiplasticizer below $T_g$ due to the existence of the bulky phenylene rings with limited molecular mobility. As for further discussion of the effect of BPA, it should be necessary to characterise the mixing state of BPA with noncrystalline PET segments.

## CONCLUSIONS

Detailed $^2H$ n.m.r. analysis has been carried out for different phenylene-deuterated PET samples at a wide range of temperatures to characterise the phenylene motions in different regions included, and the following conclusions have been obtained.

(1) $^2H$ spin-lattice relaxation processes are described in terms of three components with different $T_1$ values at −30–130°C in slowly cooled PET, quenched PET, and quenched PET containing 10 wt% bisphenol-A. These three components are assigned to the crystalline, less mobile noncrystalline, and mobile noncrystalline components in the order of decreasing $T_1$ value.

(2) By considering the $T_1$ relaxation process, some equations for the magnetizations are derived as functions of the time for relaxation to separately record $^2H$ n.m.r. spectra of the respective components. According to these equations the total $^2H$ n.m.r. spectra are successfully resolved into the crystalline, total noncrystalline, and mobile noncrystalline components at different temperatures for each sample.

(3) $^2H$ n.m.r. spectra thus obtained for the respective components are in good accord with the spectra simulated with the two-site 180° flip model by introducing log-Gaussian distributions in flip rate which reflect the characteristic phenylene motions in the respective components.

(4) Average correlation times of the flip motions and mass fractions, which are both obtained by the above simulation of the $^2H$ n.m.r. spectra, are shown for the respective components as a function of temperature in each sample. On the basis of these results, it is found that the less mobile and mobile noncrystalline components, which are different in flip frequency by 100–1000 Hz, are significantly changed in mass fraction and flip frequency depending on the PET samples.

(5) BPA is effective as plasticizer of PET above $T_g$, probably owing to the rapid phenylene flip motion, whereas it plays a role as antiplasticizer below $T_g$ due to the hindered flip motion.

## REFERENCES


1. Eichhoff, V. and Zachmann, H.G., *Kolloid Z. Z. Polym.*, 1970, **241**, 928.
2. English, A.D., *Macromolecules*, 1984, **17**, 2182.
3. VanderHart, D.L., Bohm, G.G.A. and Mochel, V.D., *Polym. Prepr. Am. Chem Soc. Div Polym. Chem.*, 1981, **22**(2), 261.
4. Horii, F., Hirai, A., Murayama, K., Kitamaru, R. and Suzuki, T., *Macromolecules*, 1983, **16**, 273.
5. Sefcik, M.D., Schaefer, F., Stejskal, E.O and Mckay, R.A., *Macromolecules*, 1980, **13**, 1132.
6. Henrichs, P.M., Tribone, J. and Massa, D.J., *Macromolecules*, 1988, **21**, 1282.
7. Komoroski, R.A., *J. Polym. Phys. Ed.*, 1979, **17**, 45.
8. Cholli, A.L., Dumais, J.J., Engel, A.K. and Jelinski, L.W., *Macromolecules*, 1984, **17**, 2399.
9. Gehrke, R., Gulibrzuch, M., Klaue, A. and Zachmann, H.G., *Polym. Prepr. Am Chem. Soc. Div. Polym. Chem.*, 1988, **29**(1), 64.
10. Hirschinger, J., Miura, H., Gardner, K.H. and English, A.D., *Macromolecules*, 1990, **23**, 2153.
11. Miura, H., Hirschinger, J. and English, A.D., *Macromolecules*, 1990, **23**, 2169.
12. Schmidt, C., Kuhn, K.J. and Spiess, H.W., *Progr. Colloid Polym. Sci.*, 1985, **71**, 71.
13. Wehrle, M., Hellmann, G.P. and Spiess, H.W., *Colloid Polym. Sci.*, 1987, **265**, 815.
14. Horii, F., Beppu, T., Takaesu, N. and Ishida, H., *Magn. Reson. Chem.*, 1994, **32**, S30.
15. Mehring, M., *Principles of High Resolution NMR in Solids*, 2nd edn., Springer-Verlag, New York, 1983.
16. Horii, F., Uyeda, T., Beppu, T., Murata, T. and Odani, H., *Bull. Inst. Chem. Res. Kyoto Univ.*, 1992, **70**, 198.
17. Gall, C.M., DiVerdi, J.A. and Opella, S.J., *J. Am. Chem. Soc.*, 1981, **103**, 5039.
18. Bloom, M., Davis, J.H. and Valic, M.I., *Can. J. Phys.*, 1980, **58**, 1510.
19. Spiess, H.W. and Sillescu, H., *J. Magn. Reson.*, 1981, **42**, 381.
20. Hosokawa, Y., Amiya, T., Yasuda, Y., Kawaguchi, T. and Horii, F., *Polym. Prepr. Jpn.*, 1992, **41**(9), 3779.
21. Havens, J.R. and VanderHart, D.L., *Macromolecules*, 1985, **18**, 1663.
22. Kimura, T., Neki, K., Tamura, N., Horii, F., Nakagawa, M. and Odani, H., *Polymer*, 1992, **23**, 493.
23. Ishida, M., Yoshinaga, K. and Horii, F., *Macromolecules*, 1996, **29**, 8824.